Highly sensitive potentiometric pH sensor based on polyaniline modified carbon fiber cloth for food and pharmaceutical applications

Md. Sanwar Hossain[a,c], Narayanasamy Padmanathan[b], Mizanur R. Badal[a], Kafil M. Razeeb[b*] and Mamun Jamal[a*]

[a]Department of Chemistry, Khulna University of Engineering & Technology, Khulna 9203, Bangladesh

[b]Micro-NanoSystems Centre, Tyndall National Institute, University College Cork, Dyke Parade, Lee Maltings, Cork T12 R5CP, Ireland

[c]Current workplace: Institute of National Analytical Research and Service (INARS), Bangladesh Council of Scientific and Industrial Research (BCSIR), Dhanmondi, Dhaka 1205, Bangladesh

[*]Corresponding author email: mamun.jamal@chem.kuet.ac.bd, and kafil.mahmood@tyndall.ie

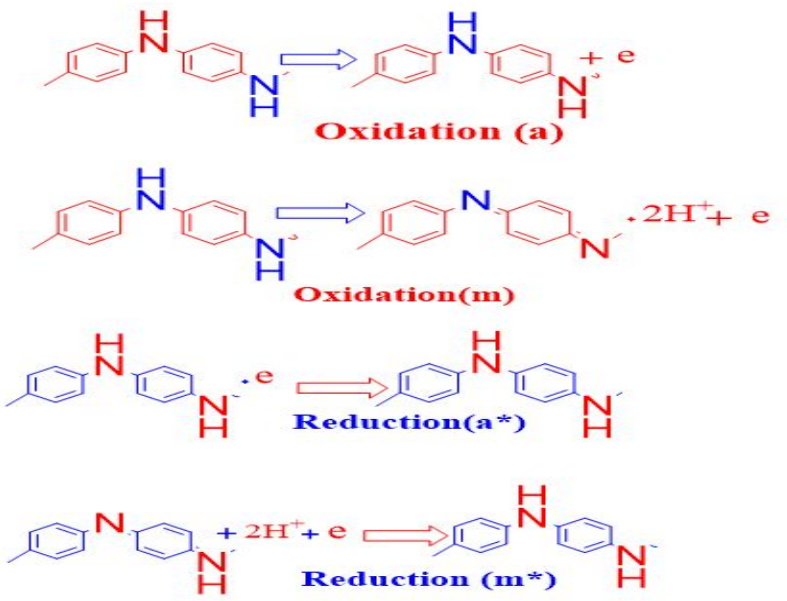

Figure S1. Protonation and deprotonation of polyaniline (PANI).

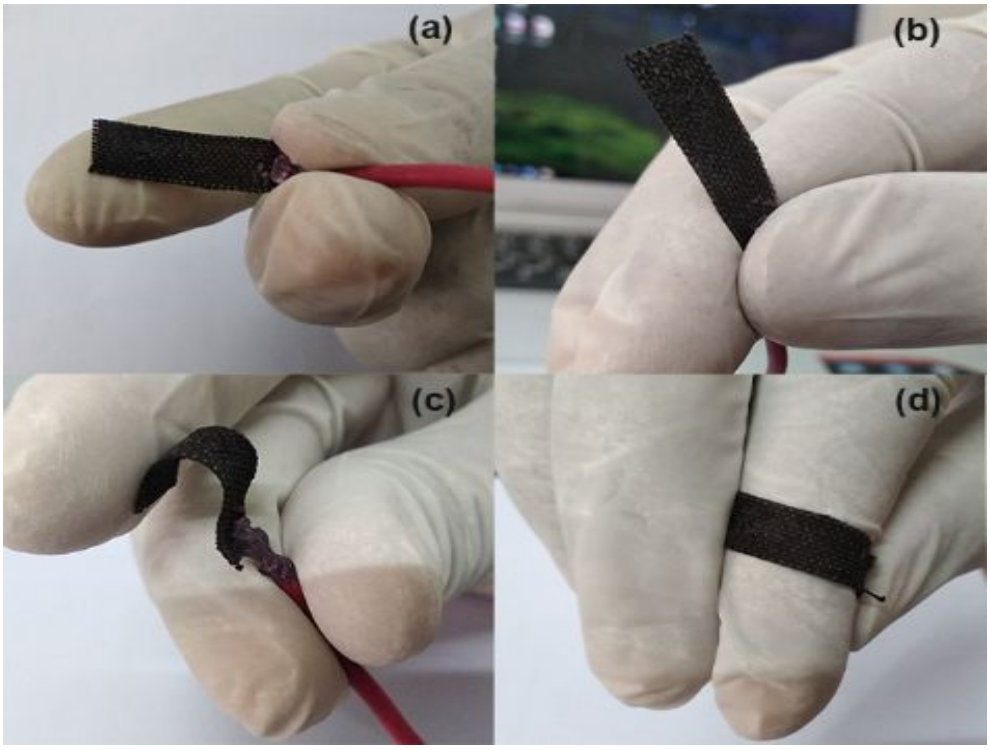

Figure S2. PANI modified CFC Electrodes (a-d).

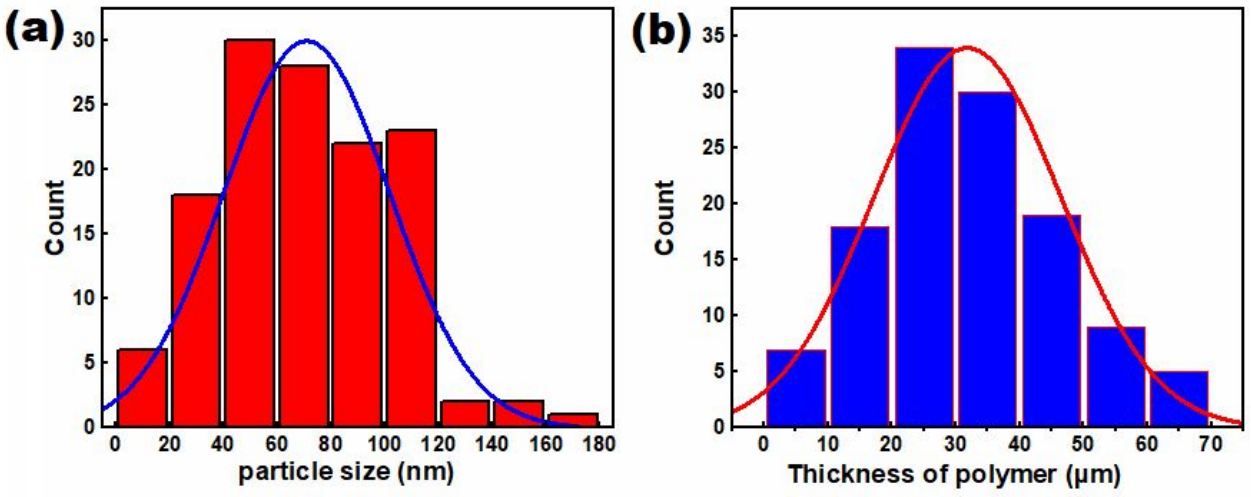

Figure S3. (a) Distribution curve of PANI on CFC; and (b) distribution curve of cross section thickness of PANI.

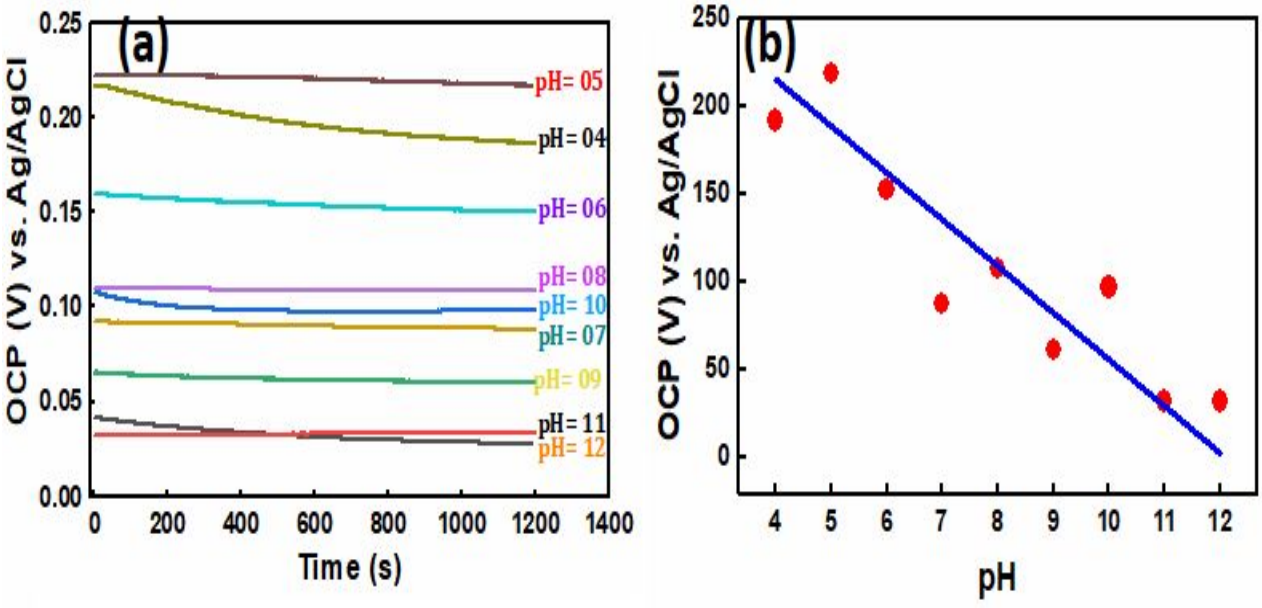

Figure S4. (a) Potential response of CFC at different pH (4–12) in 0.1 M buffer solution; and (b) the corresponding linear relation plot.

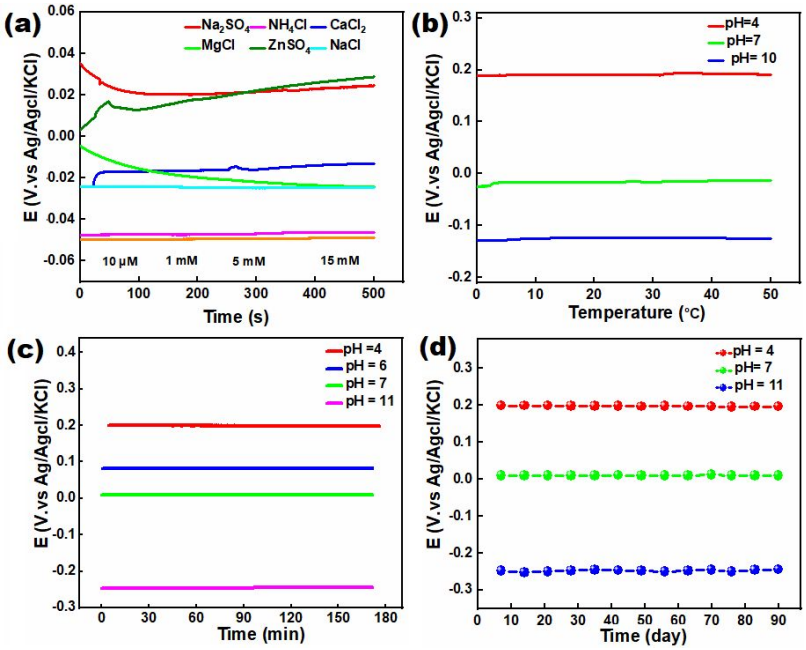

Figure S5 (a) Interference behavior of the PANI/CFC sensor in the presence of six common interfering ions of varying concentrations from 10 µM to 15 mM in water; (b) measured pH sensor potential as a function of temperature for different pH values of 4, 7, and 10; (c) drift behavior of the pH sensor for 3h at pH 4, 7 and 11; (d) drift behavior of the pH sensor for 3 moth at pH 4, 7 and 11.

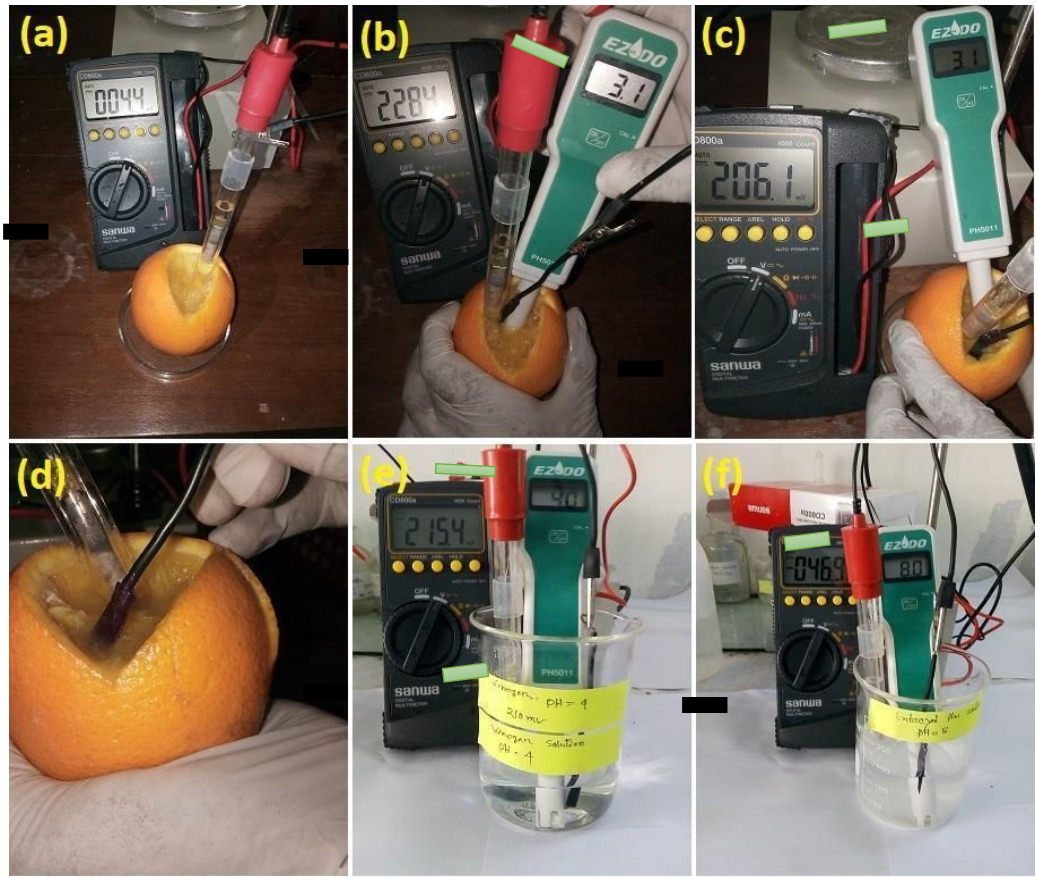

Figure S6. Real sample test images of (a-d) malta; (e) vinegar; and (f) antacid plus.

Table S1. Repeatability of PANI-CFC electrode at room temperature.

Serial NO:	Electrode Name	pH range	Sensitivity (mV/pH)
1	PANI-CFC	4-12	60.9
2	PANI-CFC	4-12	63.3
3	PANI-CFC	4-12	64.2
4	PANI-CFC	4-12	60.7
5	PANI-CFC	4-12	63.8

S1. Optimized geometry and Interaction energy calculation using DFT

The geometries of deprotonated and protonated PANI (emeraldine base) were Optimized at the DFT-B3LYP/6-311+G (d, p) level of theory. The optimized structure of the smallest modeled oligomer consists of four repeating units of PANI, as illustrated in Supplementary Figure S7.

$$\Delta E_{int} = E_{reactant1} + E_{reactant2} - E_{product} \quad \textit{Equation 1}$$

The energies of the deprotonation and protonation of PANI were calculated at the same level of theory, as shown in Supplementary Table S1. This method was employed for interaction energy measurements, and the interaction energy was calculated using equation 1 [1, 2]. The interaction energy of PANI-2H+ was -173.2886 kcal/mol. This large value of the interaction energy is also in agreement with the experimental data, which illustrates the selectivity of conducting polymers towards H+. The optimized geometrical parameters, including the bond lengths, bond angles, and dihedral angles of 4PANI, are listed in Supplementary Table S2 and Supplementary Figure S7. The bond lengths and angles that are directly associated with the reaction site undergo the most considerable changes during the sensing process. These parameters have been discussed in terms of their interactions with protons. The reason for this gradual decrease in the intramolecular bond distance is the variation in the partial positive and partial negative charges on the indicated hydrogen and nitrogen atoms, respectively, involved in this bond. When attached to protons, the partial positive and negative charges on the respective atoms vary in such a manner that the polarity of the covalent bond increases and, ultimately, a gradual reduction in most of the bond length occurs. This variation in charge is due to the pronounced flow of electronic charge from the

increasing number of protons added to PANI, the central nitrogen atom, to intensify the partial negative charge on nitrogen [3]. This is also supported by the Mulliken charge data of deprotonated and protonated PANI in the charge analysis. An increase in the bond lengths of N42-H3, N44−H45, N47−C4, N46−C1, and N42−C31, and a decrease in the bond lengths of N46−C11, N44−C18, N44−C21, and N42−C28 are observed in deprotonated PANI attached to hydrogen ions, as shown in Figure S7 (a-b) and Table S2. The increase in the N42-H3, N44−H45, N47−C4, N46−C1, and N42−C31 bond lengths is the result of protonation with an analyte, which weakens the bonds. This indicates that PANI has greater attraction towards H+ ions. The increase in bridging angle ∠C31−N42−C28, ∠C21−N44−C18, ∠C11−N46−C1, ∠C13−C11−N46, and ∠N46−C1−C2 and decrease in bridging angle C6−C1-N46, ∠C12−C11−N46, and ∠C5−C4-N47 are observed in deprotonated PANI attach with analysts (H^+) in Figure S7 (a-b). The zigzag structure causes a decrease in the bridging angle in large polymer structures [2]. The dihedral angles ∠C36−C33−C31−N42 and∠C26−C23−C21−N44 showed a consistent increase with the addition of protons, and the complexation of analytes also had a prominent effect on the geometric parameters of PANI. The sensor is specific and selective for the analyte, with which the complexation process results in the most pronounced changes in the geometric parameters. In the current study, H had a strong influence on the variation of geometric parameters on complexation, and the amount of charge transfer between 4PANI (sensors) and analytes was simulated at the B3LYP/6-311G+(d, p) level of theory. The analytes change the electronic properties of 4PANI through charge transfer. This charge transfer alters the resistance, bandgap, and λ_{max} of 4PANI, which are measurements of the sensitivity of the interaction. Mulliken charges analysis of isolated and analyte (H^+) bound nPANI complexes are given in (Supplementary Table S2) and Figure S8 (a-b). Interaction in PANI-2H^+ complexes is established due to the transfer of electrons from analysts to 4PANI, especially near the adjoining phenyl rings and bridging NH groups of 4PANI, as shown in Table S2, including some exceptions [1]. Green indicates negative to positive, as shown in Figure S8 (a-b). In protonated PANI (4PANI-2H^+), Nitrogen N46 loses about 0.2e− charge to 4PANI based on Mulliken charge analysis, which means that before reacting with H+, the phenyl rings (4) have 0.467 e−, and when reacting with H^+, the charges on these rings are reduced to 0.033 e−. Charge transfer in protonated PANI (PANI-2H^+) also decreases with chain length elongation; this phenomenon is also consistent with the results of the geometric and energetic analyses. For example, H^+ (H49) loses 0.672 e− (based on Mulliken) when H^+ is added

to the PANI. The charge transfers ability of nPANI-H^+ was calculated to study the potential of 4PANI-H^+ as a pH sensor, as shown in Figure S8 (a-b). The total charge on a ring is calculated as the sum of the charges found on all six carbons of the ring and the directly attached hydrogen atoms [1]. These rings are designated as 1, 2, 3, and 4 in Figure S8 (a-b) and represent the central pair of rings in all the modeled PANI samples. Mulliken charge analysis revealed deprotonated phenyl ring charges of 0.34 (1) e −, 0.588 (2) e −, 0.495 (3) e −, and 0.467 (4) e −. In addition, protonated phenyl ring charges were observed at 0.361(1) e−, 0.347(2) e−, 0.247 (3) e−, and 0.033(4) e−. The calculated results demonstrate that atomic electronegativity plays a vital role in Mulliken charge distribution [4]. In the current study, the analyte had a positive charge. The transfer of positive charge from the analyte to the sensor is responsible for the change in conductivity upon interaction with H^+. H^+ ions transferred charge to the sensor, resulting in a greater difference in conductivity. This is also in agreement with the experimental evidence.

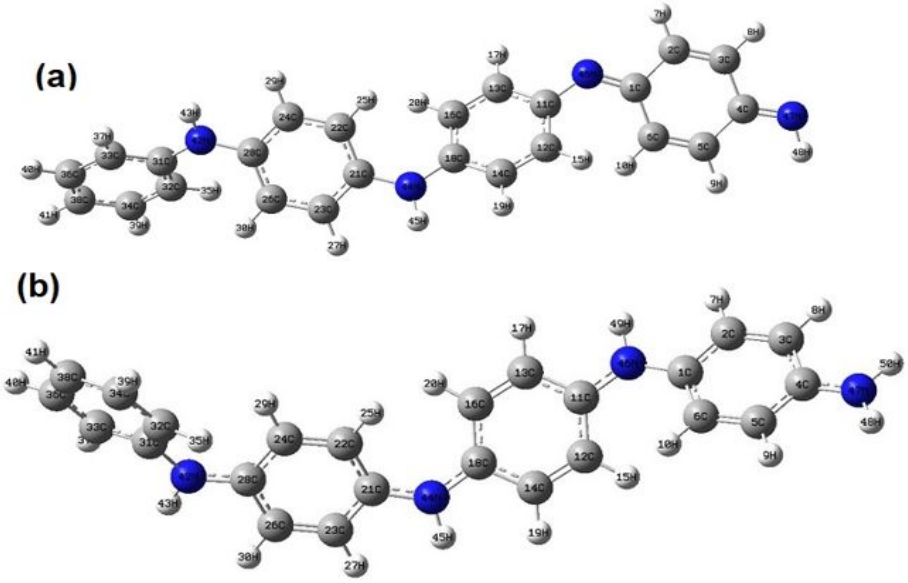

Figure S7. Optimized geometry of normal (a) deprotonated PANI; and (b) protonated PANI-$2H^+$.

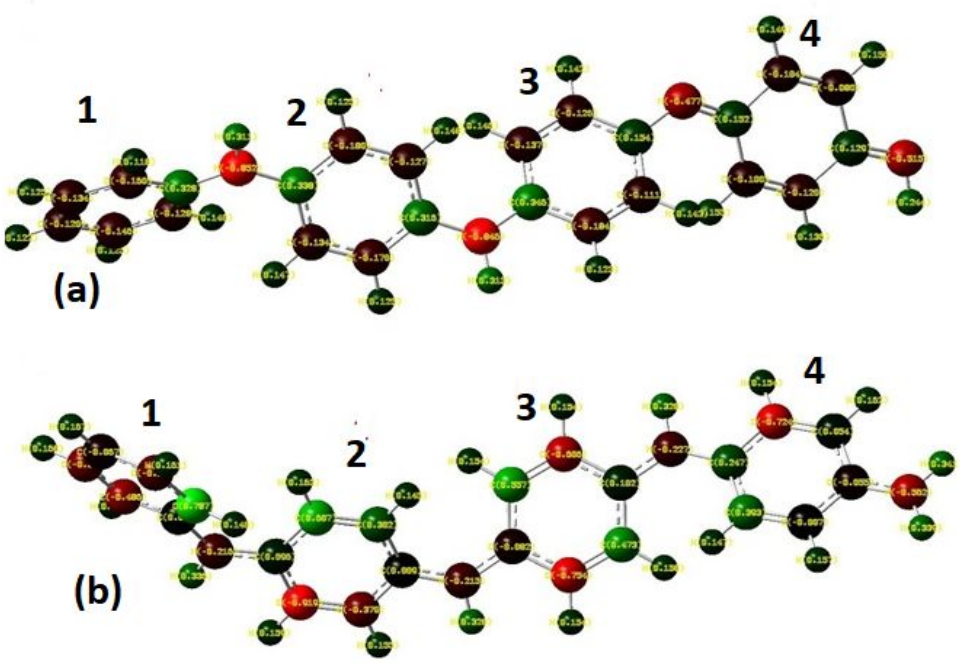

Figure S8. Mulliken charge analysis of (a) deprotonated; and (b) protonated.

S2. Vibrational studies

The IR spectra of O-PANI were calculated at the DFT/6-311G+(d, p) level of theory and scaled by 0.9688 [5], which showed good agreement with the experimental FTIR spectra. Subsequently, O-PANI-$2H^+$ IR spectra were computed to assess the changes in the peak caused by protonation. The findings are listed in Table S1, and the computed IR spectra of PANI and O-PANI-$2H^+$ are presented in Supplementary Figure S9. A few extra peaks were observed in the vibrational spectra of the 4PANI-H^+ complex, which were absent for 4PANI (Supplementary Figure S9). Interaction with H^+ not only causes the appearance of new signals, but also a considerable shift in the positions of some existing peaks. These additional peaks correspond to the coordination bonds between H^+ and PANI. The sharp secondary amine band of O-PANI-$2H^+$ shifted to 3589 cm−1 compared with the O-PANI amine peak at 3450 cm^{-1}.

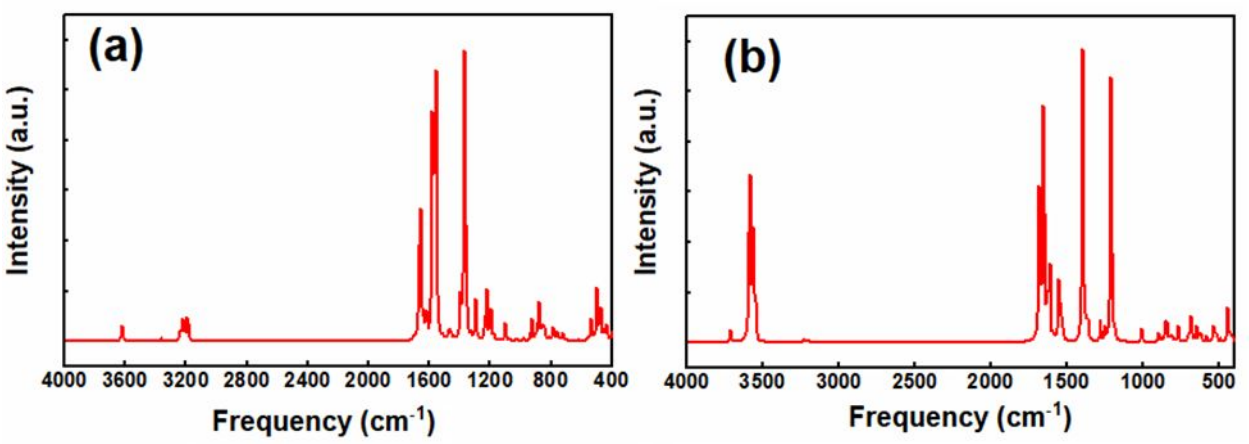

Figure S9. (a) IR spectrum of deprotonated; and (b) protonated PANI.

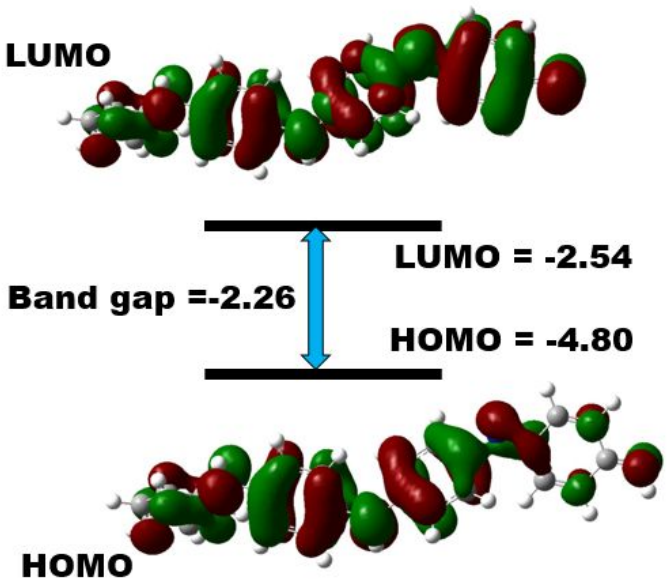

Figure S10. Frontier orbitals of deprotonated PANI and DFT B3LYP/6-311G+(d,p) level of theory.

Table S2. Energy calculation of normal PANI, proton (H^+) and PANI-$2H^+$.

Species	**E (Hartree)**	**E (Kcal/mol)**
PANI	-1,145.8582	-719037.0067
H^+	-0.5022	-315.1077
PANI+$2H^+$	-1,146.8625	-719667.2222
PANI-$2H^+$	-1,146.5863	-719493.9335

Table S3. Selected Bond Lengths, Bond Angles, and Dihedral Angles of Compounds deprotonated and protonated Calculated at the APFD/6- 311+G(d, p) Level of Theories.

Bond distances (Å)	**Deprotonated PANI**	**Protonated PANI**	**Bond angle (°)**	**Deprotonated PANI**	**Protonated PANI**
N47−C4	1.30665	1.34763	C31−N42−C28	128.959	130.751
N46−C1	1.33152	1.38601	C21−N44−C18	128.581	133.037
N46−C11	1.39594	1.36779	C11−N46−C1	126.390	132.335
N44−C18	1.39494	1.37222	C13−C11−N46	117.037	117.671
N44−C21	1.41424	1.37979	N46−C1−C2	116.750	117.390
N42−C28	1.40595	1.35875	C6−C1N−46	126.613	123.709
N42−C31	1.40574	1.41174	C12−C11−N46	125.245	123.904
N47−H48	1.03174	1.01028	C3−C4−N47	118.555	120.783
N44−H45	1.00984	1.01629	C5−C4N−47	125.151	120.754
N42−H43	1.00949	1.05151	**Dihedral angle (°)**		

N46−H49		1.01611	C36−C33−C31−N42	177.760	178.368
N47−H50		1.01045	C26−C23−C21−N44	176.956	179.652
			C16−C13−C11−N46	178.406	-179.696
			C6−C5−C4N−47	178.201	-179.476

Table S4. Mulliken charge transfer from analyte to the sensor.

Number of rings	**Deprotonated PANI(Mulliken charge)**	**protonated PANI (Mulliken charge)**	**Number of atoms**	**Deprotonated PANI(Mulliken charge)**	**protonated PANI(Mulliken charge)**
1	0.340	0.347	N47	-0.515	-0.568
2	0.588	0.347	N46	-0.477	-0.227
3	0.495	0.247	N44	-0.846	-0.215
4	0.467	0.033	N42	-0.852	-0.216
			H48	0.244	0.332
		-0.568	H45	0.314	0.329
		-0.227	H43	0.311	0.336
		-0.215	H49		0.328
		-0.216	H50		0.341

		0.332	C2	-0.104	-0.724
		0.329	C6	-0.120	0.393
		0.336	C13	-0.126	-0.606
		0.328	C14	-0.184	-0.754
		0.341	C16	-0.137	-0.575
		-0.724	C26	-0.134	-0.919
		0.393	C24	-0.180	0.607
		-0.606	C32	-0.126	0.787
		-0.754	C33	-0.166	-0.530

Table S5. Band gaps in terms of difference of HOMO and LUMO of deprotonated PANI protonated PANI.

Species	**HOMO (eV)**	**LUMO (eV)**	**Band gap (eV)**
Deprotonated PANI	-4.80	-2.54	-2.26
Protonated PANI	-10.56	-9.68	-0.98

References

1. Ullah, H. Shah, A. U. H. A. Bilal, S. and Ayub, K., 2013, "DFT study of polyaniline NH3, CO2, and CO gas sensors: Comparison with recent experimental data", *Journal of Physical Chemistry C*, Vol. 117, pp. 23701–23711.
2. Farooqi, B. A. Yar, M. Ashraf, A. Farooq, U. and Ayub, K., 2020, "Polyaniline

emeraldine salt as selective electrochemical sensor for HBr over HCl : a systematic density functional theory study through oligomer approach", *Journal of Molecular Modeling*, Vol. 26, p. 332.

3. Badal, M. M. R. Ashekul Islam, H. M. Maniruzzaman, M. and Abu Yousuf, M., 2020, "Acidochromic behavior of dibenzylidene cyclohexanone-based bischalcone: Experimental and theoretical study", *ACS Omega*, Vol. 5, pp. 22978–22983.
4. Kumar, A. Srivastava, A. K. Gangwar, S. Misra, N. Mondal, A. and Brahmachari, G., 2015, "Combined experimental (FT-IR, UV-visible spectra, NMR) and theoretical studies on the molecular structure, vibrational spectra, HOMO, LUMO, MESP surfaces, reactivity descriptor and molecular docking of Phomarin", *Journal of Molecular Structure*, Vol. 1096, pp. 94–101.
5. Merrick, J. P. Moran, D. and Radom, L., 2007, “Synthesis and characterization of cyano and iocyano complexes of bis(dithiolate) molybdenum using Me3SiCN: a route to multimer to monomer”, *Journal of Physical Chemistry A,* Vol. 111, pp. 11683–11700.